

Near-field measurement of amplitude and phase in silicon waveguides with liquid cladding

Maurice Ayache,^{1,*} Maziar P. Nezhad,¹ Steve Zamek,¹ Maxim Abashin,^{1,2} and Yeshaiah Fainman¹

¹Department of Electrical and Computer Engineering, University of California, San Diego, 9500 Gilman Drive, La Jolla, California 92093-0407, USA

²Center for Nanoscale Science and Technology, National Institute of Standards and Technology, Gaithersburg, Maryland 20899, USA

*Corresponding author: mayache@ucsd.edu

Received November 29, 2010; revised March 30, 2011; accepted April 1, 2011; posted April 15, 2011 (Doc. ID 138649); published May 13, 2011

Heterodyne near-field scanning optical microscopy (H-NSOM) has proven useful as a tool for characterization of both amplitude and phase of on-chip photonic devices in air, but it has previously been unable to characterize devices with a dielectric overcladding, which is commonly used in practice for such devices. Here we demonstrate H-NSOM of a silicon waveguide with a liquid cladding emulating the solid dielectric. This technique allows characterization of practical devices with realistic refractive index profiles. Fourier analysis is used to estimate the effective refractive index of the mode from the measured data, showing an index shift of 0.08 from air to water cladding, which is seen to correspond well to simulations. © 2011 Optical Society of America

OCIS codes: 180.4243, 130.2790.

In recent years near-field scanning optical microscopy (NSOM) [1,2] has emerged as an important characterization tool for nanoscale and microscale optical structures. By using a subwavelength probe to couple evanescent waves to a far-field detection system, the NSOM offers the dual benefits of resolution below the diffraction limit and imaging confined modes of photonic devices. Whereas traditionally, characterization of guided-wave devices would be limited to transmission/reflection measurements in the far field, NSOM enables local detection of optical fields propagating within such devices. Although fabrication and simulation technology have improved steadily, numerous defects, such as etch roughness, proximity effect, and underetching, contribute in unpredictable or poorly quantifiable ways to device performance, making their incorporation into simulations impractical. Therefore, local characterization techniques are necessary to fully understand device operation and properties. Even though NSOM analysis depends on a probe placed in proximity to the optical mode suggesting a perturbative effect, the measured fields correspond well to those in absence of the probe for nonresonant structures [3]. NSOM can be significantly improved by integration into one of the arms of a heterodyne interferometer [4–7], which allows simultaneous near-field detection of amplitude and phase. Capability of phase measurement is essential for characterization of chip-scale photonic devices, such as interferometers, modulators, and nonlinear components.

Photonic integrated circuits are typically coated with a solid overcladding to improve symmetry, protect the sample, and allow deposition of successive layers. Conventional near-field characterization of such circuits must be done without this cladding since it prevents the NSOM probe from accessing the evanescent fields at the core-cladding boundary. With no cladding, however, numerous devices lose or change their functionality, making such characterization deviate from the performance of the final device. Here we demonstrate a technique that allows optical near-field characterization of devices while preserving their optical properties. To

do so, a liquid cladding is introduced to emulate the actual cladding of the final operational device while allowing the probe to sample the fields at the core-cladding boundary for NSOM analysis. NSOM has previously been applied in a liquid environment for characterization of biological samples [8–10]. A significant contribution was made by Ji *et al.* [11] who used the NSOM to measure the intensity profile of a waveguide with a liquid overcladding. However, to date there has been no heterodyne near-field imaging of a waveguide with a liquid overcladding, which is essential due to the effect of cladding on phase.

In this Letter we measure amplitude and phase of air- and liquid-clad waveguides in the near field and then use Fourier analysis of the complex field to obtain the effective index difference between them. To the best of our knowledge, this is the only heterodyne NSOM technique that allows characterization of fully clad complex photonic circuits as a part of the fabrication and validation process. As a proof-of-concept, we consider a silicon waveguide, resting on top of a silicon dioxide substrate, with a liquid cladding, as shown in Fig. 1(a). Such a configuration serves as a canonical example for many chip-scale device and circuit designs in numerous material systems.

Characterization of the waveguide is done with a heterodyne near-field microscope (H-NSOM) [12]. The heterodyne interferometer has a Mach–Zehnder arrangement with an acousto-optic modulator in each of the two arms, with the difference between the modulation frequencies producing an RF beat in the detected optical

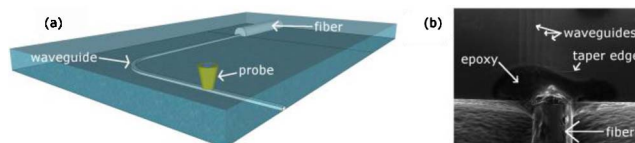


Fig. 1. (Color online) (a) Schematic of the experiment. An aperture NSOM probe scans a silicon waveguide, which is bonded to a polarization-maintaining single-mode fiber. The entire apparatus is submerged in water. (b) Scanning electron micrograph of the fiber bonded to the chip.

intensity at the output, which is sent to a lock-in amplifier. The lock-in reference frequency is set to the beat frequency, which allows the lock-in amplifier to detect the amplitude and phase. A schematic of this experiment depicting the probe, waveguide, and fiber is shown in Fig. 1(a). The NSOM itself is a Nanonics MultiView (MV) 1000 with a liquid cell module that enables full probe and sample immersion in a liquid environment. This permits simultaneous acquisition of topographic and optical data. The MV-1000 is based on sample-scanning, as opposed to probe-scanning, which makes it impossible to use a static optical fiber for coupling. Instead, in order to preserve alignment during sample motion, the fiber must be rigidly bound to the waveguide.

The waveguides are fabricated by standard e-beam lithography of hydrogen silsesquioxane (HSQ) resist on a silicon-on-insulator wafer, followed by reactive ion etching of the silicon and buffered oxide etching to remove the HSQ mask. Each waveguide is comprised of a 500 nm wide by 250 nm tall silicon ($n = 3.48$) channel on top of a silicon dioxide ($n = 1.46$) substrate buried oxide layer. The pattern produced after etching is a set of these waveguides with a 90° bend, with a taper [13] at each end. The input taper deconfines the propagating mode for improved coupling and tolerance for misalignment due to epoxy shrinkage during curing, while the output taper reduces Fresnel backreflection due to effective index mismatch. The wafer is then singulated by dicing and cleaving. The newly formed chip is mounted in a fiber-based transmission setup, where a single-mode polarization-maintaining fiber is bonded to the tapered waveguide end with low-shrinkage UV-cured epoxy (Dymax OP-20), as shown in Fig. 1(b). The fiber is oriented with the electric field vertical to the chip plane in order to excite the quasi-TM waveguide mode, which is favorable to NSOM characterization due to its long vertical evanescent decay.

We measured the waveguide at 1550 nm wavelength with the H-NSOM using a 200 nm metal-coated aperture probe, with overlappings of air and water. The waveguide is raster-scanned beneath the probe, with the fast (x) axis 25 μm long, parallel to the guide. The height, amplitude, and phase are collected at each point in the 128 \times 128 point grid. The results for this experiment with water overcladding are shown in Fig. 2. In addition to the raw topography, amplitude A and phase ϕ , we also show the calculated $A \sin \phi$, which is the imaginary part of the complex electric field propagating along the waveguide, i.e., the optical field distribution at a particular time. Despite the presence of the water, the measured waveguide height matches closely to the design, and the overall profile is similar to that recorded without any water. The amplitude plot displays a weak modulation due to reflection (<1% intensity) of the mode at the waveguide output.

To evaluate quantitatively the effect of the water, Fourier analysis is applied to each set of amplitude and phase maps. For amplitude A and phase ϕ , using the fast Fourier transform (FFT) along the x axis on Fig. 2, we calculate the estimated power spectral density $|\mathcal{F}_x\{Ae^{i\phi}\}|^2$, where x is the direction of propagation. The frequency axis is given by $n_{\text{eff}} = k\lambda_0$, where k is the FFT spatial frequency coordinate, which gives the phase spatial frequency or propagation constant. The square magnitude

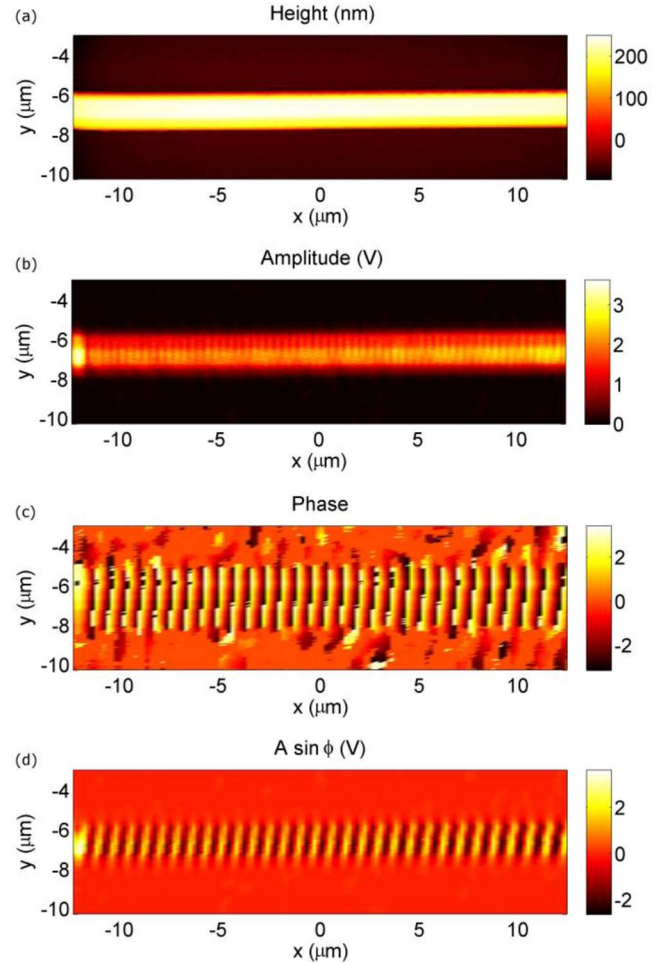


Fig. 2. (Color online) (a) Topography, (b) amplitude A , (c) phase ϕ , and (d) electric field $A \sin \phi$ maps for water overcladding.

corresponds to the power spectrum of the propagating modes. By only taking the Fourier transform along one direction, we preserve the information about the transverse distribution of the modes. To reduce spectral leakage [14] due to phase mismatch at the two ends of the scan, we remove some scan lines (corresponding to approximately 200 nm each) before performing the FFT; we remove one scan line from the data for air overcladding and two scan lines from the data for water overcladding.

Figures 3(a) and 3(b) show the power spectral density in the x direction for air and water claddings, respectively.

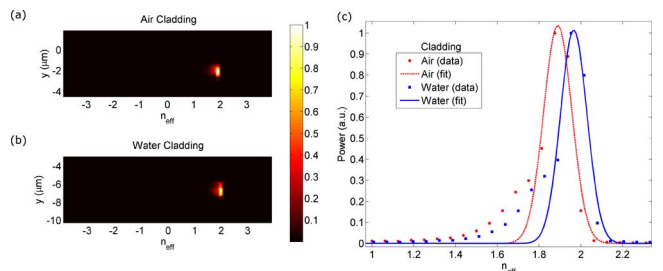


Fig. 3. (Color online) Estimated power spectral density of the optical field for (a) air and (b) water, showing a single mode in each case; (c) y -integrated data from (a) and (b), demonstrating an effective index shift of 0.08 from air to water cladding.

The horizontal coordinate gives the effective index, which increases as the cladding index is increased. The shape of the single TM mode is visible along the y axis (perpendicular to the guide), with a peak in the middle that decays evanescently to the sides. We also note that the spectral data has a low-index tail of unknown origin; further experiments are necessary to understand this effect.

By integrating the estimated power spectral density along the y axis, as shown in Fig. 3(c), and fitting it to a Gaussian distribution, we obtain the effective index at the peak of this Gaussian fit. For comparison, we also simulated the waveguide in cross section according to the design parameters with commercial finite element software (COMSOL Multiphysics) to determine the effective index of the quasi-TM mode of the designed structure. With an air overcladding, the effective refractive index obtained by analyzing the experimental data is $1.89 \pm .005$, close to the value of 1.84 obtained from the simulation. With a water overcladding, the index estimated from the experimental data is $1.97 \pm .005$, also close to the value of 1.95 predicted by the simulation. The precision is quite high due to the high signal-to-noise ratio enabled by the heterodyne setup and integration over the waveguide width; the accuracy, which determines the difference between the simulation and the experiment, is primarily affected by phase drift [4] and mechanical stability. The addition of the water causes a measured effective index shift of 0.08, $\sim 4\%$. This corresponds to a π phase difference over $\sim 10 \mu\text{m}$, less than characteristic lengths of typical silicon photonic devices, making an accurate cladding essential to preserve the phase properties of the device.

In summary, we demonstrated a technique of liquid-based heterodyne near-field characterization of photonic devices and circuits. As a proof-of-concept, we measured the full complex field (amplitude and phase) of the guided quasi-TM mode in a waveguide with air and water overcladdings. Using Fourier analysis of the measured fields we obtained the effective indices of the guided modes, which are in good agreement with the results obtained from numerical simulations. This technique opens up a number of new possibilities, including using H-NSOM as a part of photonic circuit validation during and after the fabrication process. Availability of liquids with refractive indices varying from 1.3 to 1.8 allows emulation of most solid dielectrics commonly used as a cladding. For structures with SiO_2 undercladding, using index-matching liquid at $n = 1.46$ to create a symmetric

environment would be useful in measurement of losses, as well as characterization of low-confinement fields, such as those associated with tapers and higher-order modes. Additionally, aqueous solutions would be useful for high-resolution phase-contrast imaging of biological molecules and live cells.

The authors wish to acknowledge support from the Cymer Corporation, the Defense Advanced Research Projects Agency (DARPA), the National Science Foundation (NSF) and NSF through the Engineering Research Center for Integrated Access Networks (CIAN ERC). We thank Nanonics, Ltd. for extensive training and support, Nano3 staff at the University of California, San Diego (UCSD), and Bill Mitchell at the University of California, Santa Barbara (UCSB) for e-beam lithography. Finally, we thank Dr. Boris Slutsky and Aleksandar Simic for help with the experimental setup.

References

1. A. Lewis, M. Isaacson, A. Harootunian, and A. Muray, *Ultra-microscopy* **13**, 227 (1984).
2. D. W. Pohl, W. Denk, and M. Lanz, *Appl. Phys. Lett.* **44**, 651 (1984).
3. M. Abashin, U. Levy, K. Ikeda, and Y. Fainman, *Opt. Lett.* **32**, 2602 (2007).
4. M. L. M. Balistreri, J. P. Korterik, L. Kuipers, and N. F. van Hulst, *Phys. Rev. Lett.* **85**, 294 (2000).
5. A. Nesci, R. Dandliker, H. P. Herzig, *Opt. Lett.* **26**, 208 (2001).
6. M. Abashin, P. Tortora, I. Märki, U. Levy, W. Nakagawa, L. Vaccaro, H. P. Herzig, and Y. Fainman, *Opt. Express* **14**, 1643 (2006).
7. M. Abashin, K. Ikeda, R. Saperstein, and Y. Fainman, *Opt. Lett.* **34**, 1327 (2009).
8. H. Muramatsu, N. Chiba, K. Homma, K. Nakajima, T. Ataka, S. Ohta, A. Kusumi, and M. Fujihira, *Appl. Phys. Lett.* **66**, 3245 (1995).
9. C. E. Talley, G. A. Cooksey, and R. C. Dunn, *Appl. Phys. Lett.* **69**, 3809 (1996).
10. M. Koopman, A. Cambi, B. I. de Bakker, B. Joosten, C. G. Figdor, N. F. van Hulst, and M. F. Garcia-Parajo, *FEBS Lett.* **573**, 6 (2004).
11. W. Ji, D. Kim, H. J. Kim, O. Beom-Hoan, S. Park, E. Lee, and S. G. Lee, *IEEE Photon. Technol. Lett.* **17**, 846 (2005).
12. A. Nesci and Y. Fainman, *Proc. SPIE* **5181**, 62 (2003).
13. V. R. Almeida, R. R. Panepucci, and M. Lipson, *Opt. Lett.* **28**, 1302 (2003).
14. J. M. Blackledge, *Digital Image Processing: Mathematical and Computational Methods* (Woodhead, 2005).